ARTICLE

Chirality-Resolved Length Analysis of Single-Walled Carbon Nanotube Samples through Shear-Aligned Photoluminescence Anisotropy

John P. Casey, Sergei M. Bachilo, Christine H. Moran, and R. Bruce Weisman*

Department of Chemistry, Richard E. Smalley Institute for Nanoscale Science and Technology, and Center for Biological and Environmental Nanotechnology, Rice University, 6100 Main Street, Houston, Texas 77005

ABSTRACT An efficient new method is demonstrated for measuring length distributions of semiconducting single-walled carbon nanotubes (SWCNTs) through analysis of their highly polarized photoluminescence when aligned by shear flows. Instrumentation and procedures are developed to characterize nanotube lengths in bulk suspensions with rapid data acquisition and interpretation. Applying the method with spectrally resolved SWCNT emission provides the first measurements of (*n*,*m*)-specific length distributions. A positive correlation is found between average length and nanotube diameter, although this correlation is weaker following extensive sample centrifugation. Intense sonication shortened all nanotube species and had the strongest effect on those with small diameters. The new method should provide a useful alternative to atomic force microscopy for characterizing SWCNT lengths.

KEYWORDS: single-walled carbon nanotubes · length distribution · shear alignment · photoluminescence anisotropy · near-IR fluorescence

Single-walled carbon nanotubes (SWCNTs) are an intensely studied class of artificial nanomaterials with unique optical, electronic, and mechanical properties. Numerous proposed devices exploiting these SWCNTs' properties may play significant roles in future technologies.[1,2] Such applications commonly depend on SWCNT electronic character (metallic/semiconducting), transverse structure (defined by indices (*n*,*m*)), and length. For example, relatively short nanotubes are desirable in electronic devices requiring ballistic transport,[3] whereas longer nanotubes are preferred for reinforcing composite materials.[4] Although the solution-phase manipulation of SWCNTs is advancing quite rapidly, improved tools to analyze sample length distributions are badly needed.

Optical spectroscopies, particularly photoluminescence, have been shown to be effective and practical for analyzing the diameters and chiral angles present in bulk samples.[5,6] However, length characterization is much more tedious, typically relying on the analysis of atomic force microscopy (AFM) images to compile statistically valid histograms.[7−9] Sample preparation in this approach is non-trivial, as the substrate surface generally needs chemical treatment before SWCNT deposition. There is also the possibility of systematic sampling error if the length distribution deposited onto the AFM substrate does not represent the distribution in suspension. The bulk methods of depolarized dynamic light scattering and multi-angle light scattering have been used to characterize SWCNT size distributions in liquid suspensions, although these non-resonant scattering techniques cannot distinguish between nanotubes and impurities.[10−12] In addition, light scattering analysis is complicated by the broad optical absorptions of SWCNT samples. A non-optical mechanical shear method has also recently been reported that provides average length values. This is similarly non-selective for nanotubes, as it measures viscosity contributions from all particles in the sample.[13] There is thus still a serious unmet need for a new, SWCNT-specific method that can efficiently measure length distributions of bulk nanotube samples and even resolve those distributions for different (*n*,*m*)-species.

It is well-established that SWCNTs individualized in liquid dispersion show sharp and intense optical transitions, including near-infrared photoluminescence (PL), that are highly characteristic of their (*n*,*m*) structure.[14,15] Moreover, the strong transitions are highly polarized parallel to the nanotube axis.[16] This implies that the nano-

*Address correspondence to weisman@rice.edu.

Received for review June 8, 2008 and accepted July 10, 2008.

Published online July 31, 2008.
10.1021/nn800351n CCC: $40.75

tube orientation is a major factor controlling the intensity of absorption and emission of linearly polarized light. A number of studies have used optical methods to study the orientation of carbon nanotubes aligned by mechanical stretching,[17] electric fields,[18,19] and shear in a flowing liquid.[20,21] It has been shown that optical measurements on anisotropic particles aligned by a known force can be used to extract size information.[22,23] Electric fields are often used to induce such particle orientation. However, the wide range of SWCNT polarizabilities coupled with the high conductivity of typical aqueous suspensions complicates the electric field alignment of nanotubes. Alignment through mechanical methods is simpler, since the forces involved are mainly determined by particle geometry.[24] A fluid with a nonuniform flow velocity exerts a net torque on an anisotropic particle, leading to alignment of its major axis along the flow direction. This effect has recently been used for opto-mechanical size characterization of microscopic systems such as amyloid fibrils.[25] SWCNTs are a prime candidate for related orientational analysis methods because of their large aspect ratios and highly anisotropic optical properties.

We present here a method for characterizing semiconducting SWCNTs in fluid suspension using length analysis by shear-aligned photoluminescence anisotropy (LASAPA). Instrumentation is described that measures the optical anisotropy of carbon nanotubes in shear flows. We also present a theoretical approach for analyzing the measured data to obtain the distribution of nanotube lengths present in the sample. The validity of the LASAPA method is tested by comparison to AFM results. In addition, we use the method with spectrally resolved emission to study (*n*,*m*)-dependent changes in nanotube length distributions induced by sonication and centrifugation processing. Our results show that sonication preferentially shortens smaller diameter SWCNTs. We believe that the new method is the first one capable of revealing nanotube length distributions with selectivity in (*n*,*m*)-structure.

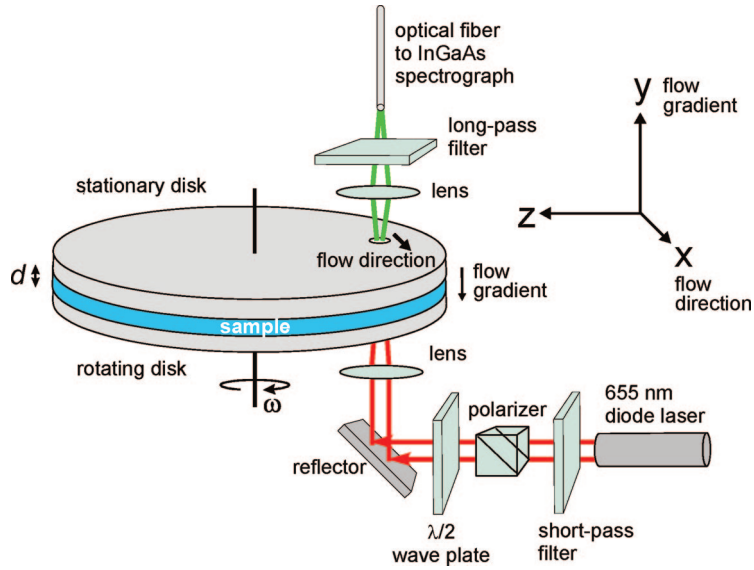

Figure 1. Optical schematic of instrument for measuring polarized photoluminescence of SWCNTs under shear flow. The laser polarization is purified and oriented before focusing into the sample volume. SWCNT near-IR emission is collected and delivered to a spectrograph/InGaAs photodiode array. The sample shear rate is controlled by the sample gap, *d* (adjustable from ~50 to 2000 μm), the distance between rotation axis and observation window (7.2 mm), and the rotating disk angular velocity ω (up to 10 rad/s).

RESULTS AND DISCUSSION

Steady-state photoluminescence anisotropy of aqueous SWCNT suspensions in a shear flow is measured using a custom-made apparatus sketched in Figure 1. Briefly, the instrument consists of a commercial optical shear cell with adjustable gap and rotation rate containing a sample of suspended SWCNTs. The sample is excited with a diode laser, the polarization of which is controlled using a linear polarizer followed by a half-wave retardation plate. Near-infrared emission from the SWCNT sample is collected by a small-aperture lens and analyzed by a photodiode array mounted on a spectrograph. (See Experimental Section for details.)

As illustrated in Figure 2, the velocity gradient (shear) in the sample cell partially aligns SWCNTs along the direction of flow, labeled *X*. When the excitation beam, which propagates along the *Y*-axis, is polarized parallel to the *X*-axis, nanotube absorption is increased by this alignment and emission is intensified. We detect the spectrally resolved emission intensity in the *Y* direction without polarization selection. Rotating the excitation beam polarization by 90° (from *X* to *Z*) gives a shear-induced decrease in sample emission because the nanotubes absorb less strongly after partial alignment. However, this effect is nearly canceled by an increase in emission detection efficiency as SWCNTs tend to align perpendicular to the detection direction (within

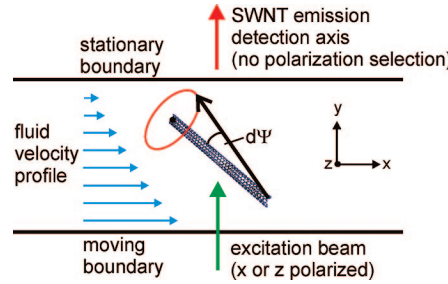

Figure 2. Illustration of a nanotube in a linear shear flow. The shear rate γ is equal to the velocity of the moving boundary divided by the distance between the two windows. Rotational diffusion is visualized as a small random change, dψ, in the angle of the nanotube axis. The exciting light beam propagates along the *Y*-axis, and a small collection aperture is used to collect *X*- and *Z*-polarized emission in the forward direction.

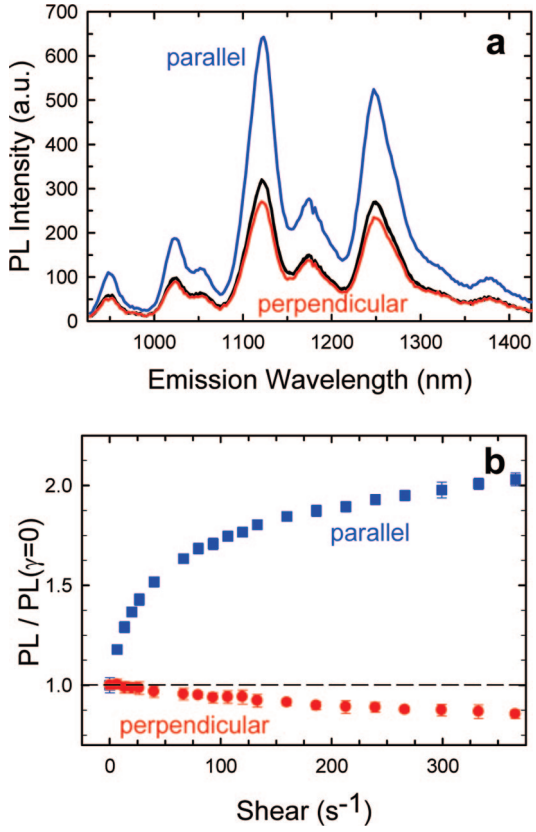

Figure 3. Emission spectra (a) and shear profiles (b) for a SWCNT suspension. In (a), the black curve was measured with no shear, and the red and blue curves were measured with a shear rate of 330 s^{-1} (blue, excitation polarized parallel to flow direction; red, excitation polarized perpendicular to flow direction). PL intensities in (b) were integrated from 925 to 1425 nm, measured at discrete shear rates, and normalized to the zero-shear value.

the $X-Z$ plane). The spectra of Figure 3a illustrate these spectral intensity changes for a SWCNT sample dispersed in aqueous surfactant, measured for both polarization settings with and without shear. The smooth dependence of PL intensity on shear and the high precision displayed in Figure 3b suggest the potential for deducing SWCNT length distributions by quantitatively fitting such "shear profiles" to an appropriate theoretical model.

Extraction of length information requires knowledge of how SWCNTs align in a flow field and how that degree of alignment can be deduced from the optical measurements. We treat the surfactant-coated nanotubes as rigid rods in the dilute regime $C < \langle L^{-3} \rangle$, where C is the number concentration and L is rod length. This is a reasonable approximation in our samples, where $\langle L \rangle < 1$ μm and $C \sim 10^{17}$ m^{-3} for mass concentrations of a few milligrams per liter.[26] In this dilute case, interactions between rods may be neglected as we consider the motions of individual rods under simple shear. The steady-state rotational diffusion equation for this system has no simple analytical solution.[27] Therefore, we take a molecular dynamics approach and numerically simulate the rotational trajectories of rods exposed to two competing effects: orientational randomization by rotational Brownian motion, and alignment by the fluid velocity gradient. We use the classical theory developed by Jeffery to model the shear-induced orientation of a rigid rod.[28] The angular rotation of a prolate ellipsoid experiencing flow in the X direction with a linear gradient in the Y direction is described by the following differential equations (in spherical coordinates, with azimuth θ measured from Z-axis and equatorial angle φ in the $X-Y$ plane measured from the Y-axis):

$$d\phi = \frac{\gamma}{R^2+1}(R^2 \cos^2\phi + \sin^2\phi)\, dt$$
$$d\theta = \gamma \frac{R^2-1}{R^2+1} \sin\theta \cos\theta \sin\phi \cos\phi\, dt \qquad (1)$$

Here, γ is the shear rate (dv_x/dy) and R is a geometric parameter that equals 1.35 times the aspect ratio for thin rods. For the large aspect ratios relevant here, both lines of eq 1 become nearly independent of R. Over a short time interval dt, rotational diffusion causes the following angular change dψ in a rod's orientation:

$$d\psi = 2\sqrt{D_r\, dt} \qquad (2)$$

Note that the direction of this step dψ is random, giving a final orientation vector lying along the red circle drawn in Figure 2. The rotational diffusion coefficient D_r is given by

$$D_r = \frac{3k_B T(\ln(L/D) - 0.8)}{\pi \eta L^3} \qquad (3)$$

where k_B is the Boltzmann constant, T is the temperature, L and D are the rod's hydrodynamic length and diameter, and η is the fluid viscosity.[29] It is clear from eq 3 that, for the large aspect ratios of our SWCNTs (for which $L > 100$ nm and $D \cong 5$ nm including surfactant layer), rotational diffusion is strongly dependent on length but nearly independent of diameter. By contrast, the flow alignment described by eq 1 is proportional to shear rate γ but nearly independent of length L. By iteratively applying these formulas for small steps over long times, we numerically simulated the time-averaged, orientation-dependent optical parameters of a SWCNT for a range of chosen lengths and shear rates (see Supporting Information).

We assume that the dominant transition dipoles for SWCNT emission and absorption lie parallel to the nanotube axis.[30] For linearly polarized excitation along the X-axis and unpolarized detection in the Y-direction, the PL intensity from a nanotube of length L subjected to shear rate γ can then be written:

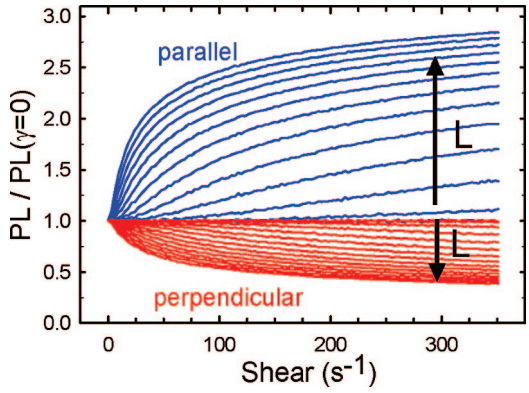

Figure 4. Simulated shear profiles for parallel (blue) and perpendicular (red) excitation polarization as a function of applied shear. Curves were computed as described in the text. The arrows denote increasing nanotube lengths from 300 to 2900 nm in 200 nm steps.

$$I(\gamma,L) \propto \langle X^2 \sigma (X^2 + Z^2) \Phi_{PL} \rangle \quad (4)$$

where X, Y, and Z designate the length- and shear-dependent nanotube projections along laboratory-fixed Cartesian axes (with $X^2 + Y^2 + Z^2 = 1$), σ is the parallel-polarized absorption cross section at the excitation wavelength, and Φ_{PL} is the photoluminescence quantum yield. The length dependence of SWCNT absorptivities and quantum yields is currently controversial.[31−33] If the optical response of the nanotubes increases non-linearly with length, then our method would overestimate the value of $\langle L \rangle$. However, we assume here that, within the studied range of lengths, σ is proportional to L and Φ_{PL} is a constant for each (n,m) species. This assumption appears to be supported by the consistency of $\langle L \rangle$ values deduced from our method and from AFM analysis (see below).

In real, polydisperse samples, the experimentally measured emission intensity should equal the summed contributions from all nanotube lengths present, weighted by their relative number concentrations. $I(\gamma,L)$ form a set of basis functions that can be used to model the total intensity emitted by the polydisperse sample at shear rate γ. Figure 4 plots the numerical simulations (see Experimental Section for details) of these basis functions for lengths ranging from 300 to 2900 nm in 200 nm steps. The computed traces resemble the experimental data in Figure 3b for both parallel and perpendicular excitation polarizations. We model the experimentally measured shear profiles as

$$I_{exp}(\gamma) = \kappa \int_{L_{min}}^{L_{max}} f(L)\, I(\gamma,L)\, dL \quad (5)$$

where κ is a proportionality constant, $f(L)$ is the length number distribution function, and the integration limits cover all lengths significantly present in the sample.

Because the basis functions $I(\gamma,L)$ are found from numerical simulation, we approximate the integral in eq 5 as a sum over a set of N discrete lengths, indexed by n, evaluated at a larger number of shear rates, indexed by m:

$$I_{exp}(\gamma_m) = C \sum_{n=1}^{N} f(L_n)\, I(\gamma_m, L_n) \quad (6)$$

Least-squares fitting to the experimental data in this over-determined system provides the discrete relative length distribution, $f(L_n)$. Additional restrictions on $f(L)$ can be imposed to ensure continuity of the distribution (*e.g.*, by assuming a specific functional form).[9] However, as we have no *a priori* knowledge of the distribution's shape, we require only that $f(L)$ cannot be negative.

The black squares in Figure 5a show the spectrally integrated PL intensity for a SWCNT−surfactant dispersion as a function of shear rate. The middle and top frames of Figure 5b compare the length distribution deduced from fitting this integrated shear profile and a length histogram found from AFM analysis of 149 SWCNTs from the same sample. (The broad first bar represents the total abundance of nanotubes shorter than

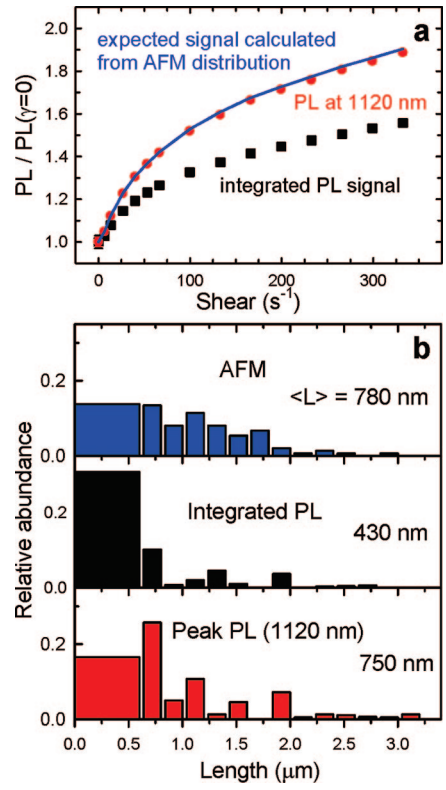

Figure 5. Comparison of LASAPA and AFM length analyses. (a) Shear profile data measured for spectrally integrated (black squares) and 1120 nm (red circles) emission. (b) Length histograms and average lengths for the same SWCNT sample obtained from AFM image analysis of 149 nanotubes (top panel), from the spectrally integrated shear profile (middle panel), and from the 1120 nm shear profile (bottom panel). The wide bars between 0 and 550 nm represent relative abundances of SWCNTs that were too short to resolve. The blue trace in (a) shows the shear profile predicted from the AFM data.

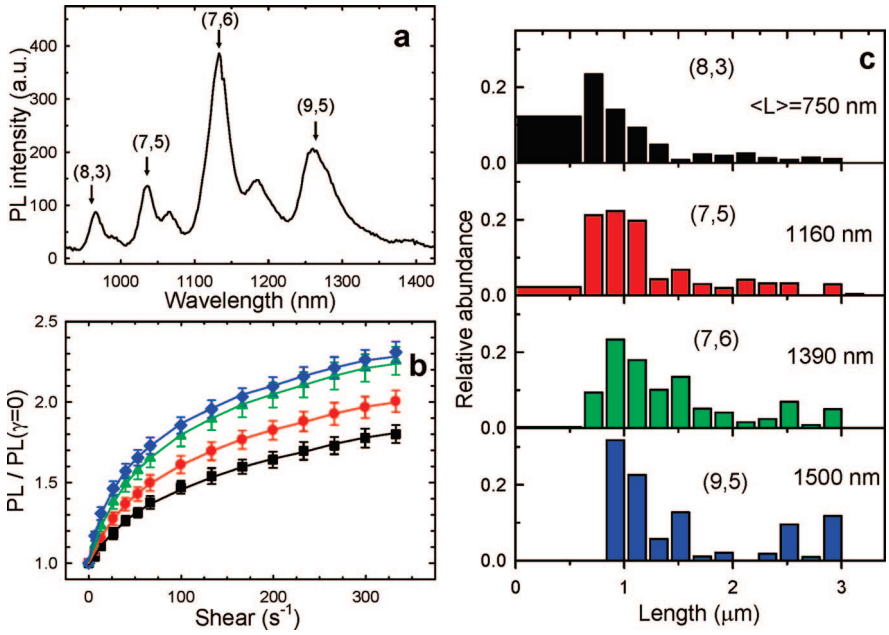

Figure 6. Structure-resolved length analysis. (a) Emission spectrum showing four (*n*,*m*) prominent peaks that were measured to give the shear profiles shown in (b) (top to bottom: (9,5), (7,6), (7,5), and (8,3)). (c) Length histograms and average lengths deduced from analysis of the shear profiles in (b).

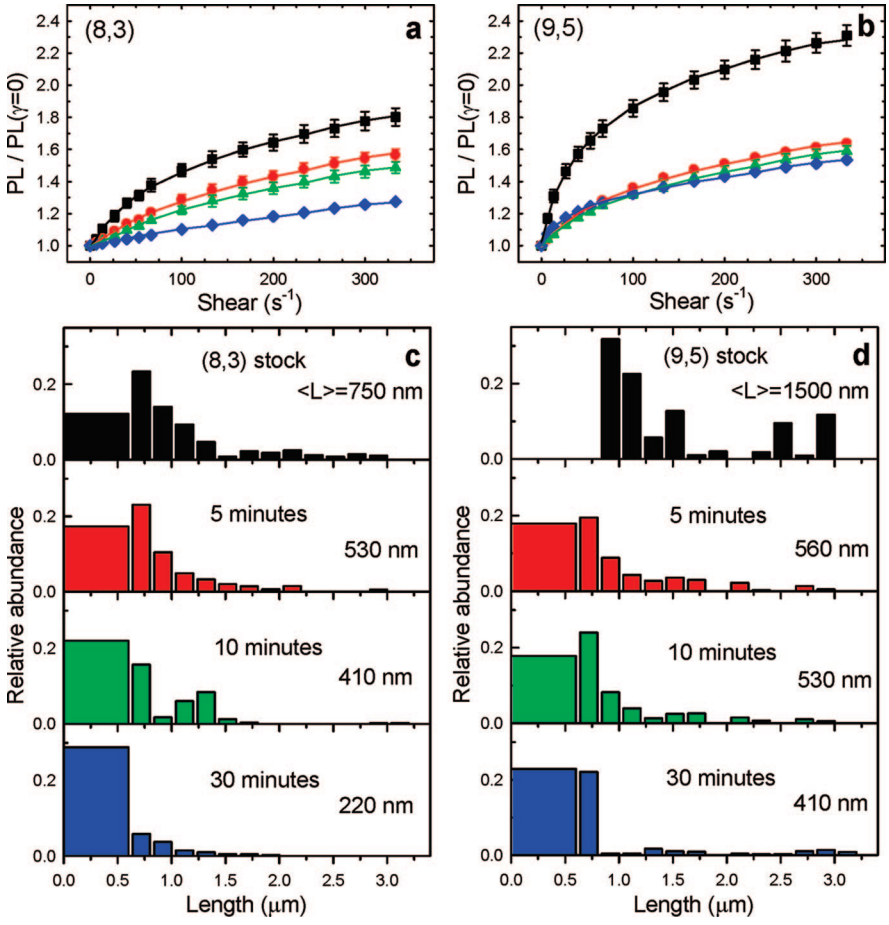

Figure 7. Effect of additional high-power sonication. Shear profiles measured (a) for (8,3) and (b) for (9,5) SWCNTs after 0, 5, 10, and 30 min (top to bottom) of additional sonication. (c,d) Length distributions and average lengths deduced from the data in (a) and (b).

550 nm, which were unresolved in this analysis.) The average length deduced from the shear alignment method (with spectral integration) is 430 nm, a value significantly below the 780 nm average length found using AFM. We believe that this discrepancy arises mainly from non-zero absorption cross sections for light polarized perpendicular to the nanotube axis. This depolarization effect can reflect the intrinsic electronic structure of isolated SWCNTs or extrinsic processes such as energy transfer among nearby or bundled nanotubes. Depolarization artifacts are expected to be greatest when SWCNTs are excited off-resonance but should be minimal for those (*n*,*m*) structures that have E_{22} transitions nearly resonant with the excitation laser and give the strongest near-IR emission features. Analysis of the shear profile measured only from the strongest spectral peak at 1120 nm is shown in the bottom frame of Figure 5. We note that the average length from this analysis is 750 nm, in very good agreement with the AFM value. (The standard deviation for average length determinations with our method is typically 50 nm.) As a further check of consistency between the LASAPA and AFM results, we have used the AFM length distribution as $f(L_n)$ in eq 6 to simulate an experimental shear profile. The solid curve in Figure 5a shows this parameter-free simulation, which agrees extremely well with the resonantly excited shear profile data.

As the entire PL spectrum of the sample is measured simultaneously in the LASAPA method, one can find separate length distributions for specific (*n*,*m*) structures. Using PL intensities at the four prominent emission peaks labeled in Figure 6a, we have measured the shear profiles shown in Figure 6b on a "stock" sample different from that used for Figure 5. Although these peaks contain minor amplitude components from other (*n*,*m*) species, they are dominated by the indicated structures, which are excited near resonance by the 655 nm laser. These SWCNTs vary in di-

ameter from 0.782 nm (8,3) to 0.976 nm (9,5) and in chiral angle from 15.3° (8,3) to 27.46° (7,6). Although it is difficult to uncover trends in chiral angle and diameter based on only four SWCNT types, the data in Figure 5c suggest that the larger diameter nanotubes in our samples are longer. Despite a diameter difference of less than 0.2 nm, the (8,3) nanotubes in this sample have an average length only half that of the (9,5) nanotubes (~750 *vs* ~1500 nm). Such diameter-dependent length distributions would be very difficult to discern by AFM.

To test the ability of the LASAPA method to reveal changes in length distributions from sample processing, we exposed portions of our stock sample to 5, 10, or 30 min of additional tip sonication at ~50 times greater power density than used for initial dispersion. Shear profiles and corresponding length distributions for the small-diameter (8,3) and large-diameter (9,5) SWCNTs are shown in Figure 7. Increased sonication time results in lower abundances of long SWCNTs. In addition, it can be seen that the (8,3) nanotubes show a shorter average length than the (9,5) nanotubes at all sonication durations and do not show the limiting behavior apparent for (9,5). This difference might be explained by recent reports that SWCNT sonication breakage can be described using polymer scission theory.[34,35] In this view, the collapse of microscopic bubbles generated by cavitation produces intense radial flow that exerts high tensile forces along the nanotube axis. The force necessary to break a nanotube into two equal fragments would be proportional to diameter, leading to a prediction of greater fracture probability for smaller diameter species.

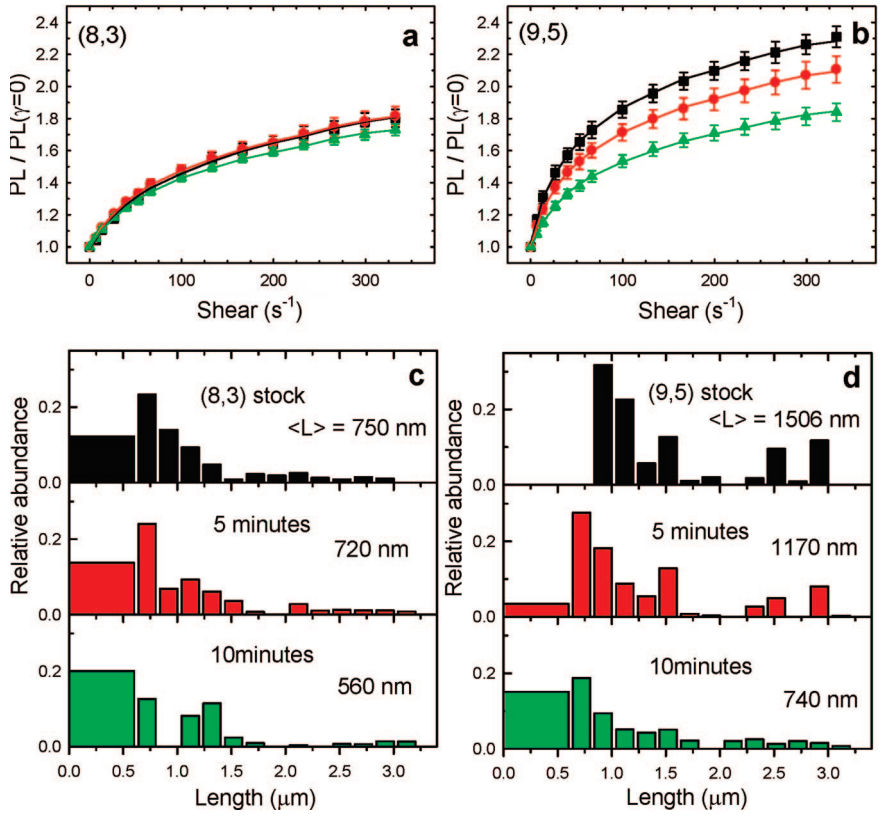

Figure 8. Effect of additional centrifugation. Shear profiles measured (a) for (8,3) and (b) for (9,5) SWCNTs after 0, 5, and 10 min (top to bottom) of additional centrifugation. (c,d) Length distributions and average lengths deduced from the data in (a) and (b).

Another effect to consider is the aggregation of SWCNTs.[36,37] Although most bundles are unlikely to emit because of the presence of metallic nanotubes, some small bundles will luminesce and contribute to our data. The bundle content may be significant because of the relatively weak centrifugation used in our initial sample preparation. Some small bundles will contain staggered nanotubes and have lengths greater than their isolated components. If sections of these bundled SWCNTs emit, their lengths could be overestimated in our measurements. Another bundle-related process, energy transfer between SWCNTs,[38] could lead to diameter-dependent PL effects. The downhill migration of energy within a bundle of semiconducting nanotubes would result in quenching of small-diameter (large band gap) nanotubes and enhanced PL from large-diameter species.[39,40] Such bundles with long hydrodynamic lengths would then be interpreted as large-diameter SWCNTs in our spectrally resolved measurements. It appears, however, that the effects suggested above are in fact minor, because our AFM data for the sample shown in Figure 5 gave an average length decrease of only 15% when possible bundles (comprising half of the measured features) were excluded. It is therefore likely that the strong variation of average length with diameter seen in Figure 6 mainly reflects the actual distribution of single-nanotube lengths in the sample.

We also examined the effect of centrifugation on SWCNT length distributions (Figure 8). The stock sample was centrifuged at 8500*g* for an additional 5 and 10 min. In general, the average length decreased with increasing centrifugation time for all (*n*,*m*) species in the decanted fraction. We found that the length distribution deduced for smaller diameter SWCNTs was somewhat changed by centrifugation, while SWCNTs of larger diameter became substantially shorter. The average (9,5) length remained longer than that of (8,3) at all centrifugation times, but the relative difference between them decreased. As shown in Figure 9, these trends continued when the sample was extensively ultracentrifuged (4 h at ~120000*g*). The diameter dependence of average length was much weaker in the strongly centrifuged sample, which showed a relative

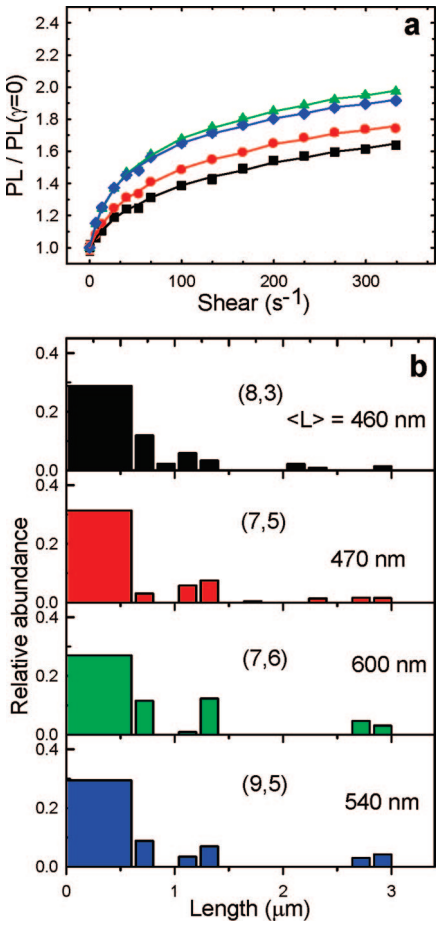

Figure 9. Comparison of length distributions for different (*n*,*m*) species after ultracentrifugation for 4 h at 120000*g*. (a) Shear profiles for (7,6), (9,5), (7,5), and (8,3) (top to bottom). (b) Length distributions and average lengths deduced from the data in (a).

⟨*L*⟩ variation of only 27% compared to 63% with weak centrifugation.

As mentioned earlier, our LASAPA experimental conditions allowed alignment only of nanotubes at least ~500 nm long. SWCNTs below this length remained essentially unaligned at accessible shear rates and therefore contributed no anisotropy to the PL signal, preventing resolution of the length histogram below 550 nm. To gain information about these shorter nanotubes, we increased the sample viscosity by adding glycerol. This viscosity increase slows rotational Brownian motion (see eq 3) and thus allows greater nanotube alignment at a given shear rate. In Figure 10, we compare the shear profiles and length distributions for (8,3) nanotubes in a sonication-shortened, well-dispersed sample in water and in 80 wt % glycerol (viscosity ~50 times that of water).[41] It is clear that the viscous medium provides significantly more shear-induced optical anisotropy from short SWCNTs. The average lengths deduced from the two shear profiles are identical within their precisions, but the length distribution can be resolved for much shorter nanotubes in the viscous medium. We find that the SWCNTs shorter

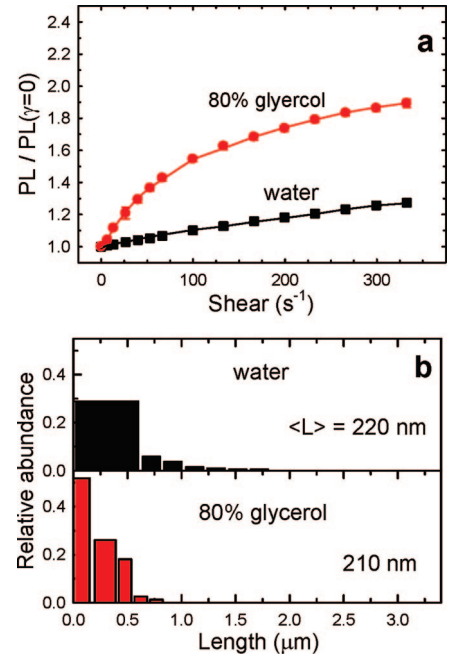

Figure 10. Improved length resolution from LASAPA method in a higher viscosity medium. (a) Shear profiles measured for (8,3) emission in water (black squares) and in 80 wt % glycerol (red circles) The sample was shortened by 30 min sonication, as shown in Figure 7. (b) Length distributions and average lengths deduced from the data in (a).

than 550 nm are distributed as ~17% from 350 to 550 nm, ~26% from 150 to 350 nm, and ~53% below 150 nm in length. We note that accurate viscosity measurements are needed when using media with high glycerol contents for this application.

Ideally, a characterization method should not alter the sample, so one might question whether our shear conditions changed the SWCNT length distribution. In our most extensive measurements, we sheared the sample for approximately 1 h while rotation rates were cycled for signal averaging. Some samples showed decreasing anisotropy early in the run but then stabilized to a highly reproducible level. (Error bars are drawn in all plots and are typically smaller than the data symbols.) In general, these initial changes were minor and are believed to be caused by dissociation of weakly bound aggregates into individual nanotubes.

In conclusion, we have demonstrated a new optical method (LASAPA) based on near-IR PL for determining the (*n*,*m*)-resolved length distributions of semiconducting SWCNTs as they are aligned by fluid shear in aqueous suspensions. Data collection and analysis in this method can be significantly faster than for AFM (as short as 10 min) and provide comparable average length measurements, although resolution of length distributions below ~500 nm currently requires the use of high-viscosity media. We observe clear evidence of nanotube shortening by intense sonication treatment, particularly for small-diameter SWCNTs. In addition, there is a persistent positive correlation between average nanotube length and diameter in the studied samples. Although PL is highly ef-

fective in selecting against impurities and resolving the properties of different chiral species in a sample, it cannot be used with SWCNTs that are substantially aggregated, covalently functionalized, or metallic. Our approach may be adapted to other optically anisotropic processes such as absorption, birefringence, or Raman scattering to probe such species. We believe that refinements to instrumentation and data analysis will let the LASAPA method evolve into a practical tool for characterizing nanotube lengths with unprecedented selectivity.

EXPERIMENTAL SECTION

Optical Instrument. The layout for the analytical instrument is shown in Figure 1. Approximately 1 mL of SWCNT solution is placed into a commercial optical shear cell (Linkam Scientific CSS450). The shear cell consists of two quartz windows separated by an adjustable gap d with liquid sample between them. One window is fixed while the other rotates at angular frequency ω. A small aperture at a radius $r = 7.2$ mm is used for sample observation. The small detection region allows the shear rate to be linearly approximated as $\gamma = r\omega/d$. A gap of 200 μm was typically used with rotation rates of up to 10 rad/s.

The sample was excited by a 655 nm diode laser beam (through a Schott KG3 filter). The beam's polarization was purified with a Glan polarizer and oriented with a half-wave plate before being focused into the sample cell with a 30 mm f.l. lens. The SWCNT emission was collected on the opposite side of the cell using a small-aperture lens and delivered to an InGaAs spectrograph (CVI SM302) by an optical fiber. A long-pass Schott RG830 filter was used to block stray laser light from entering the collection fiber. PL spectra were recorded as a function of shear rate. At each shear rate, the system was allowed a few seconds to equilibrate before measurements were recorded.

Materials. Raw HiPco single-walled carbon nanotubes were obtained from Rice University's Carbon Nanotechnology Laboratory and dispersed in 1% aqueous sodium dodecyl benzenesulfonate (SDBS) as previously reported,[42] except with milder tip sonication (5 W power for 1 h applied to 100 mL sample volume) and weaker centrifugation (5000*g* for 10 min). Tapping-mode AFM (Veeco Nanoscope) was performed on samples spin-coated on mica and washed with isopropyl alcohol and *n*-methylpyrrolidone. Simagis image analysis software (Smart Imaging Technologies) was used to obtain length distributions from AFM data.

Simulations. The equations of motion in the text were integrated using an iterative program which simulates the rotational motion of a nanotube of specific length under defined shear conditions over 10^8 time steps of 1 μs. In each iteration, the nanotube made a small random angular step (eq 2) and was then reoriented according to eq 1 for the given length, shear, and initial angles (see Supporting Information). Very small time steps of 1 μs guaranteed that the simulation resolved rotational dynamics to about 1°, even for shorter SWCNTs. Simulated optical data as a function of length and shear were computed by calculating the appropriate time-averaged projections of the SWCNT orientation onto laboratory axes. (The earliest 10% of each trajectory was ignored to remove any dependence on initial conditions.) Values obtained in this way constitute the basis functions of eq 4. For the lengths considered here, the random rotational diffusion removes any dependence of the final functions on initial orientation, so it was not necessary to compute ensemble averages.

Acknowledgment. This research was supported by the Welch Foundation (C-0807), the NSF (CHE-0314270 and CHE-0809020), the NSF Center for Biological and Environmental Nanotechnology (EEC-0647452), and Applied NanoFluorescence, LLC.

Supporting Information Available: Analytical expressions used in the numerical simulation of nanotube orientation in shear flows. This material is available free of charge *via* the Internet at http://pubs.acs.org.

REFERENCES AND NOTES

1. Avouris, P.; Chen, J. Nanotube Electronics and Optoelectronics. *Mater. Today* **2006**, *9*, 46–54.
2. Coleman, J. N.; Khan, U.; Gun'ko, Y. K. Mechanical Reinforcement of Polymers Using Carbon Nanotubes. *Adv. Mater.* **2006**, *18*, 689–706.
3. Javey, A.; Guo, J.; Paulsson, M.; Wang, Q.; Mann, D.; Lundstrom, M.; Dai, H. J. High-Field Quasiballistic Transport in Short Carbon Nanotubes. *Phys. Rev. Lett.* **2004**, *92*, 106804.
4. Laborde-Lahoz, P.; Maser, W.; Martinez, T.; Benito, A.; Seeger, T.; Cano, P.; de Villoria, R. G.; Miravete, A. Mechanical Characterization of Carbon Nanotube Composite Materials. *Mech. Adv. Mater. Struct.* **2005**, *12*, 13–19.
5. Belin, T.; Epron, R. Characterization Methods of Carbon Nanotubes: A Review. *Mater. Sci. Eng. B—Solid State Mater. Adv. Technol.* **2005**, *119*, 105–118.
6. Hartschuh, A.; Pedrosa, H. N.; Peterson, J.; Huang, L.; Anger, P.; Qian, H.; Meixner, A.; Steinert, M.; Novotny, L.; Krauss, T. D. Single Carbon Nanotube Optical Spectroscopy. *ChemPhysChem* **2005**, *6*, 577–582.
7. Avouris, P.; Chen, J.; Freitag, M.; Perebeinos, V.; Tsang, J. C. Carbon Nanotube Optoelectronics. *Phys. Status Solidi B* **2006**, *243*, 3197–3203.
8. Ziegler, K. J.; Rauwald, U.; Gu, Z. N.; Liang, F.; Billups, W. E.; Hauge, R. H.; Smalley, R. E. Statistically Accurate Length Measurements of Single-Walled Carbon Nanotubes. *J. Nanosci. Nanotechnol.* **2007**, *7*, 2917–2921.
9. Wang, S. R.; Liang, Z. Y.; Wang, B.; Zhang, C. Statistical Characterization of Single-Wall Carbon Nanotube Length Distribution. *Nanotechnology* **2006**, *17*, 634–639.
10. Badaire, S.; Poulin, P.; Maugey, M.; Zakri, C. In Situ Measurements of Nanotube Dimensions in Suspensions by Depolarized Dynamic Light Scattering. *Langmuir* **2004**, *20*, 10367–10370.
11. Lee, J. Y.; Kim, J. S.; An, K. H.; Lee, K.; Kim, D. Y.; Bae, D. J.; Lee, Y. H. Electrophoretic and Dynamic Light Scattering in Evaluating Dispersion and Size Distribution of Single-Walled Carbon Nanotubes. *J. Nanosci. Nanotechnol.* **2005**, *5*, 1045–1049.
12. Bauer, B. J.; Fagan, J. A.; Hobbie, E. K.; Chun, J.; Bajpai, V. Chromatographic Fractionation of SWNT/DNA Dispersions With On-Line Multi-Angle Light Scattering. *J. Phys. Chem. C* **2008**, *112*, 1842–1850.
13. Parra-Vasquez, A. N. G.; Stepanek, I.; Davis, V. A.; Moore, V. C.; Haroz, E. H.; Shaver, J.; Hauge, R. H.; Smalley, R. E.; Pasquali, M. Simple Length Determination of Single-Walled Carbon Nanotubes by Viscosity Measurements in Dilute Suspensions. *Macromolecules* **2007**, *40*, 4043–4047.
14. Bachilo, S. M.; Strano, M. S.; Kittrell, C.; Hauge, R. H.; Smalley, R. E.; Weisman, R. B. Structure-Assigned Optical Spectra of Single-Walled Carbon Nanotubes. *Science* **2002**, *298*, 2361–2366.
15. Weisman, R. B.; Bachilo, S. M. Dependence of Optical Transition Energies on Structure for Single-Walled Carbon Nanotubes in Aqueous Suspension: An Empirical Kataura Plot. *Nano Lett.* **2003**, *3*, 1235–1238.
16. Bozovic, I.; Bozovic, N.; Damnjanovic, M. Optical Dichroism in Nanotubes. *Phys. Rev. B* **2000**, *62*, 6971–6974.
17. Kim, Y.; Minami, N.; Kazaoui, S. Highly Polarized Absorption and Photoluminescence of Stretch-Aligned Single-Wall Carbon Nanotubes Dispersed in Gelatin Films. *Appl. Phys. Lett.* **2005**, *86*, 073103.

18. Donovan, K. J.; Scott, K. Transient Electric Birefringence in Suspensions of Single-Walled Carbon Nanotubes. *Phys. Rev. B* **2005**, *72*, 195432-1–195432-8.
19. Fagan, J. A.; Bajpai, V.; Bauer, B. J.; Hobbie, E. K. Anisotropic Polarizability of Isolated Semiconducting Single-Wall Carbon Nanotubes in Alternating Electric Fields. *Appl. Phys. Lett.* **2007**, *91*, 213105-1–213105-3.
20. Fry, D.; Langhorst, B.; Kim, H.; Grulke, E.; Wang, H.; Hobbie, E. K. Anisotropy of Sheared Carbon-Nanotube Suspensions. *Phys. Rev. Lett.* **2005**, *95*, 038304-1–038304-4.
21. Fry, D.; Langhorst, B.; Wang, H.; Becker, M. L.; Bauer, B. J.; Grulke, E. A.; Hobbie, E. K. Rheo-Optical Studies of Carbon Nanotube Suspensions. *J. Chem. Phys.* **2006**, *124*, 054703-1–054703-9.
22. Morris, V. J.; Foweraker, A. R.; Jennings, B. R. Particle-Size Distributions From Transient Electric Birefringence Data. 1. Polydisperse Rods by 2-Parameter Distribution Functions. *Adv. Mol. Relax. Interact. Processes* **1978**, *12*, 65–83.
23. Morris, V. J.; Foweraker, A. R.; Jennings, B. R. Particle-Size Distribution From Transient Electric Birefringence Data. 3. Polydisperse Ellipsoids by 2-Parameter Distribution Functions. *Adv. Mol. Relax. Interact. Processes* **1978**, *12*, 211–220.
24. Rodger, A.; Marrington, R.; Geeves, M. A.; Hicks, M.; de Alwis, L.; Halsall, D. J.; Dafforn, T. R. Looking at Long Molecules in Solution: What Happens When They Are Subjected to Couette Flow. *Phys. Chem. Chem. Phys.* **2006**, *8*, 3161–3171.
25. Rogers, S. S.; Venema, P.; Sagis, L. M. C.; van der Linden, E.; Donald, A. M. Measuring the Length Distribution of a Fibril System: A Flow Birefringence Technique Applied to Amyloid Fibrils. *Macromolecules* **2005**, *38*, 2948–2958.
26. Duggal, R.; Pasquali, M. Dynamics of Individual Single-Walled Carbon Nanotubes In Water by Real-Time Visualization. *Phys. Rev. Lett.* **2006**, *96*, 246104-1–246104-4.
27. Wang, C. H.; Vugmeister, B. E.; Ouyang, H. D. Pretransitional Orientational Ordering of Rigid-Rod Polymers in Shear-Flow. *Phys. Rev. E* **1993**, *48*, 4455–4459.
28. Jeffery, G. B. The Motion of Ellipsoidal Particles Immersed in a Viscous Fluid. *Proc. R. Soc. London A* **1922**, *102*, 161–179.
29. Doi, M.; Edwards, S. F. *The Theory of Polymer Dynamics*; Oxford University Press: New York, 1986.
30. Lefebvre, J.; Fraser, J. M.; Finnie, P.; Homma, Y. Photoluminescence From an Individual Single-Walled Carbon Nanotube. *Phys. Rev. B* **2004**, *69*, 075403-1–075403-5.
31. Heller, D. A.; Mayrhofer, R. M.; Baik, S.; Grinkova, Y. V.; Usrey, M. L.; Strano, M. S. Concomitant Length and Diameter Separation of Single-Walled Carbon Nanotubes. *J. Am. Chem. Soc.* **2004**, *126*, 14567–14573.
32. Fagan, J. A.; Simpson, J. R.; Bauer, B. J.; De Paoli Lacerda, S. H.; Becker, M. L.; Chun, J.; Migler, K. B.; Hight Walker, A. R.; Hobbie, E. K. Length-Dependent Optical Effects in Single-Wall Carbon Nanotubes. *J. Am. Chem. Soc.* **2007**, *129*, 10607–10612.
33. Sun, X.; Zaric, S.; Daranciang, D.; Welsher, K.; Lu, Y.; Li, X.; Dai, H. Optical Properties of Ultrashort Semiconducting Single-Walled Carbon Nanotube Capsules Down to Sub-10 nm. *J. Am. Chem. Soc.* **2008**, *130*, 6551–6555.
34. Arnold, K.; Hennrich, F.; Krupke, R.; Lebedkin, S.; Kappes, M. M. Length Separation Studies of Single Walled Carbon Nanotube Dispersions. *Phys. Status Solidi B* **2006**, *243*, 3073–3076.
35. Hennrich, F.; Krupke, R.; Arnold, K.; Stutz, J. A. R.; Lebedkin, S.; Koch, T.; Schimmel, T.; Kappes, M. M. The Mechanism of Cavitation-Induced Scission of Single-Walled Carbon Nanotubes. *J. Phys. Chem. B* **2007**, *111*, 1932–1937.
36. Niyogi, S.; Boukhalfa, S.; Chikkannanavar, S. B.; McDonald, T. J.; Heben, M. J.; Doorn, S. K. Selective Aggregation of Single-Walled Carbon Nanotubes *via* Salt Addition. *J. Am. Chem. Soc.* **2007**, *129*, 1898–1899.
37. McDonald, T. J.; Engtrakul, C.; Jones, M.; Rumbles, G.; Heben, M. J. Kinetics of PL Quenching During Single-Walled Carbon Nanotube Rebundling and Diameter-Dependent Surfactant Interactions. *J. Phys. Chem. B* **2006**, *110*, 25339–25346.
38. Qian, H.; Georgi, C.; Anderson, N.; Green, A. A.; Hersam, M. C.; Novotny, L.; Hartschuh, A. Exciton Energy Transfer in Pairs of Single-Walled Carbon Nanotubes. *Nano Lett.* **2008**, *8*, 1363–1367.
39. Torrens, O. N.; Milkie, D. E.; Zheng, M.; Kikkawa, J. M. Photoluminescence from Intertube Carrier Migration in Single-Walled Carbon Nanotube Bundles. *Nano Lett.* **2006**, *6*, 2864–2867.
40. Tan, P. H.; Rozhin, A. G.; Hasan, T.; Hu, P.; Scardaci, V.; Milne, W. I.; Ferrari, A. C. Photoluminescence Spectroscopy of Carbon Nanotube Bundles: Evidence for Exciton Energy Transfer. *Phys. Rev. Lett.* **2007**, *99*, 137402–137404.
41. Lide D. R., Ed.; *Handbook of Chemistry and Physics*, 77th ed.; CRC Press: New York, 1997.
42. O'Connell, M.; Bachilo, S. M.; Huffman, C. B.; Moore, V.; Strano, M. S.; Haroz, E.; Rialon, K.; Boul, P. J.; Noon, W. H.; Kittrell, C.; et al. Band-Gap Fluorescence From Individual Single-Walled Carbon Nanotubes. *Science* **2002**, *297*, 593–596.